JOURNAL OF NANO- AND ELECTRONIC PHYSICS
Vol. **18** No 5, 05005(7pp) (2026)

ЖУРНАЛ НАНО- ТА ЕЛЕКТРОННОЇ ФІЗИКИ
Том **18** № 5, 05005(7cc) (2026)

OPEN ACCESS

REGULAR ARTICLE

Effect of Magnesium Doping on the Dielectric Property and Triboelectric Performance of Nanohydroxyapatite

Sindhu R L[1,2,3,*], Sini Chandran[1,3], Ananda Kumar V M[1,3,†] ✉

[1] *Mahatma Gandhi College, 695004 Thiruvananthapuram, Kerala, India*
[2] *University College, 695034 Thiruvananthapuram, Kerala, India*
[3] *University of Kerala, 695034 Thiruvananthapuram, Kerala, India*

(Received 20 April 2026; revised manuscript received 19 October 2026; published online 28 October 2026)

Hydroxyapatite, a bioceramic that mimics the mineral composition of bone, has attracted attention in both in vitro and in vivo settings for its excellent biocompatibility and osteoconductivity. Pure and magnesium-doped hydroxyapatite were synthesized using chemical method, and the samples were characterized using XRD, FTIR, and EDX. The dielectric constant, AC conductivity, dielectric loss, and capacitance of the samples were measured. The study of dielectric properties of hydroxyapatite-based materials for bioelectronics and smart biomedical devices has been a recent area of interest. Preliminary studies on the effect of these samples on the triboelectric performance of polyvinyl alcohol were also done. Magnesium is an essential trace element in human bones, and therefore, it was incorporated into the nanohydroxyapatite lattice to improve biological performance and electrical properties. The results indicate the tunability of electrical properties of nanohydroxyapatite and applications of magnesium–doped nanohydroxyapatite for future biomedical devices, sensors, and energy harvesting devices.

Keywords: Nanohydroxyapatite, Chemical precipitation, Dielectric loss, Dielectric constant, Magnesium-doped hydroxy-apatite, TENG.

DOI: 10.21272/jnep.18(5).05005 PACS numbers: 81.20.Fw, 81.07.Wx

1. INTRODUCTION

Hydroxyapatite $Ca_{10}(PO_4)_6(OH)_2$ is the primary inorganic matrix associated with human hard tissues such as bone and teeth. The fundamental properties of biocompatibility, bioactivity, osteoconductivity, and chemical resemblance to the mineral phase of bone have led to the role of hydroxyapatite in biological applications such as bone grafting, coatings for metallic implants, fillings in dentistry, and scaffolds in bone tissue engineering. Formulated at the nanoscale, nanohydroxyapatite (HA) is a promising form of hydroxyapatite, as the added surface area, resorption rate, and biointegration kinetics make it suitable for use in regenerative medicine applications [1-4]. Recently, dielectric properties associated with hydroxyapatite have been discussed for several bioelectronic interfaces, smart implants, biosensors, and drug delivery. Dielectric properties such as real permittivity (ε'), dielectric loss (ε''), and ac conductivity are the relevant material properties. The dielectric performance of hydroxyapatite composites helps to study the interactions of these materials with body tissues. Further, the dielectric properties of the HA composites can be altered to modify these interactions. By investigating these dielectric properties, novel biofunctional materials can be developed. They can respond to the signals from the body and also provide electrical stimulation to assist in the healing and regeneration of the tissues [5-7].

Magnesium (Mg^{2+}) is a trace element found in natural bone and is a known regulator of bone metabolism and mineralisation. The incorporation of magnesium into HA not only increases its biological properties but also affects its structural and electrical properties. Magnesium ions can partially substitute calcium in the crystalline lattice of HA due to their similar charge and size, resulting in total distortion of the lattice, an increased defect density, and improved ionic mobility, all of which can greatly affect the dielectric response of the material [8-10]. As such, evaluating the dielectric properties of pure and magnesium-doped nanohydroxyapatite is interesting, and it is especially important for biomedical applications, like fabricating scaffolds for bone implantation, piezoelectric coatings for surface modification of hard tissue, or smart delivery systems. The current study will consider the frequency-dependent dielectric behaviour of pure and magnesium-doped nanohydroxyapatite, synthesized by the wet chemical method, and the effect of magnesium-doped hydroxyapatite on the triboelectric performance of polyvinyl alcohol (PVA). Triboelectric nanogenerators (TENG) are important innovations in the modern period because of their sustainability, smart technologies, and renewable energy. The biomedical applications of TENGs include cell modulation, nerve stimulation, wound healing, neural prosthesis, drug delivery, hair regeneration, gene delivery, microbial disinfection, and healthcare monitoring [32]. Doping with magnesium raises lattice

* sindhuajai8@gmail.com
† Correspondence e-mail: anandmgc@gmail.com

© 2026 The Author(s). Journal of Nano- and Electronic Physics published by Sumy State University. This article is distributed under the terms and conditions of the Creative Commons Attribution (CC BY) license.

Cite this article as: Sindhu R L et al., *J. Nano- Electron. Phys.* 18 No 5, 05005 (2026) https://doi.org/10.21272/jnep.18(5).05005

strain, changes its solubility, and promotes cell differentiation and proliferation. Magnesium is the fourth most abundant trace element in human bone. Magnesium-doped nanohydroxyapatite is a promising material for enhanced bone tissue engineering, dental applications, and drug delivery systems. The present study focuses on the dielectric property of magnesium-doped nanohydroxyapatite and its effect on the triboelectric property of polyvinyl alcohol.

2. MATERIALS AND METHODS

2.1 Materials

The materials used in this study were calcium nitrate tetrahydrate, diammonium hydrogen phosphate, magnesium nitrate hexahydrate, ammonia solution, and PVA. For TENG fabrication, copper-clad plates and PTFE were used.

2.2 Synthesis and Characterisation of Nanohydroxyapatite and Magnesium-Doped Hydroxyapatite

In this study, nanohydroxyapatite was synthesized via a simple chemical precipitation method. Appropriate concentrations of calcium nitrate and diammonium hydrogen phosphate solutions were prepared with deionised water to ensure a molar ratio of calcium to phosphorus of 1.67. The reagents are mixed very slowly at a pH of 9 (using ammonia solution), and the resulting solution, on ageing, centrifuging, and heating, a dry white precipitate is obtained and is crushed to fine powder with an agate mortar [11, 12]. This powder was referred to as HA. For 5 mol % magnesium-doped sample, a suitable amount of magnesium nitrate hexahydrate is added to the calcium nitrate solution such that the (Ca + Mg)/P ratio remains 1.67. Then the entire experiment is repeated as mentioned above.

The structural analysis of the synthesised samples was done using powder X-ray diffraction. The X-ray diffraction pattern of the powdered specimen was taken using Bruker D8 ADVANCE with DAVINCI instrument operating at 30 kV and 10 mA using CuKα radiation ($\lambda = 1.5418$ Å). Diffraction patterns were collected over $10° \leq 2\theta \leq 79°$ with a step size of 0.02°. The crystallite size, lattice constants, unit cell volume, and crystallinity of the synthesised sample were determined.

The functional groups present in the sample were identified using the Fourier Transform Infrared (FTIR) Spectroscopy recorded for a wave number range of 4000 to 400 cm^{-1}. The FTIR spectra of the prepared samples were recorded by the Thermo Scientific Nicolet iS50 instrument using the KBr pellet technique.

The components in the nanohydroxyapatite were examined using EDX analysis (Carl Zeiss EVO 18 Research instrument). The dielectric properties of the samples were measured by a Broadband Dielectric Spectrometer (BDS) (NOVOCONTROL Technologies GmbH & Co., Germany, Model: Concept 80).

2.3 Fabrication of Triboelectric Layers

The triboelectric performance of hydroxyapatite was evaluated by making positive triboelectric layers using nanohydroxyapatite and PVA. The positive triboelectric layers were made by mixing the nanohydroxyapatite synthesized in the appropriate ratios with the polyvinyl alcohol solution. The polyvinyl alcohol solution was made by mixing 1g of PVA powder with 15 ml of deionized water in a magnetic stirrer at a temperature of 75 ^{0}C for an hour. For hydroxyapatite, the optimal concentration to achieve maximum output is 12.5 wt % of the HA to PVA mixture. The triboelectric layer made with PVA is labelled as PVA. The hydroxyapatite triboelectric layer labelled HA was made by mixing 12.5 weight percentages of hydroxyapatite with respect to polyvinyl alcohol, coated on cleaned, etched copper-clad electrodes (4×4 cm^2), and dried at room temperature for 24 hours. In the same way as the other sample, a triboelectric layer of magnesium-doped hydroxyapatite was also fabricated and labelled as MgHA. The negative triboelectric layer was prepared with the PTFE tape wound on copper-clad electrodes.

2.4 Measurement of Electrical Output

The fabricated negative and positive triboelectric layers were mounted on an in-house developed triboelectric tester device and operated in a vertical contact separation mode. The tester moved at 1 Hz frequency and made contact with the triboelectric layers. The TENG output was measured by a Keithley 2450 sourcemeter as shown in Fig. 1. For each sample, the output is measured for three different sets of layers, and the average value is taken.

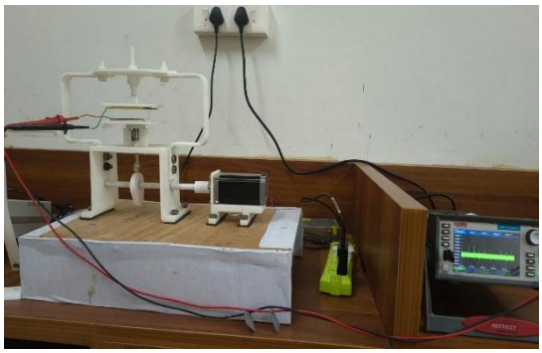


Fig. 1 – Measuring TENG output with a Keithley 2450 sourcemeter

3. RESULTS AND DISCUSSION

3.1 XRD Analysis

Fig. 2 shows the XRD pattern for pure nanohydroxyapatite and the magnesium-doped nanohydroxyapatite. The XRD pattern for nanohydroxyapatite can be indexed to the hexagonal hydroxyapatite crystal structure (ICDD No. 09-0432). Hydroxyapatite reveals its major peaks at around 25.68°, 31.5°, 32.01°, and 32.68° corresponding to (002), (211), (112), and (300) planes. There are no other peaks, which indicates that the powder is pure, and there is only one phase present. The d spacing for the strongest peak is 2.822 Å, which is consistent with a hexagonal system with a primitive lattice [11-13]. The XRD pattern of magnesium-doped hydroxyapatite is the same as that of pure hydroxyapatite. It has been observed that the peaks become wider

and shift to higher angle values with the addition of magnesium. This occurrence is due to the smaller ionic radius of magnesium (0.72 Å) when compared with that of calcium (0.99 Å), along with the increased structural strain observed in magnesium-doped hydroxyapatite compared to pure hydroxyapatite [13-14]. The presence of magnesium in hydroxyapatite leads to the creation of crystal imperfections, resulting in a more defective hydroxyapatite crystal. The broadened nature of diffraction peaks shows that the grain size of the sample was in the nanometer range. The crystallite size, lattice constants (a,c), cell volume, and crystallinity of pure and doped samples are given in Table 1.

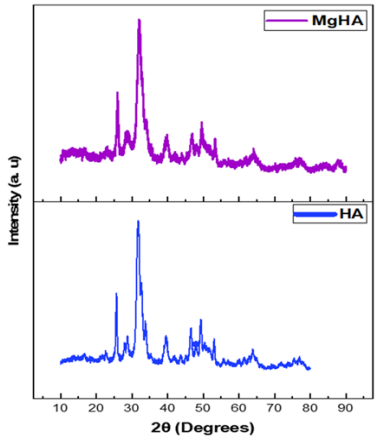


Fig. 2 – XRD pattern of HA and MgHA samples

3.2 FTIR Analysis

The FTIR Spectra for pure and magnesium-doped nanohydroxyapatite are shown in Fig. 3. Characteristic bands of hydroxyapatite were observed for phosphate, carbonate, and hydroxyl groups, as given in Table 2. The FTIR data confirms the development of hydroxyapatite [11, 18]. For the 5 mol % Mg-doped hydroxyapatite sample, the primary difference observed in FTIR spectra compared to pure HA is small shift and broadening of certain vibrational bands, particularly those associated with phosphate and hydroxyl groups. Specifically, the phosphate ($PO4^{3-}$) bands (around 560-600 cm^{-1} and 900-1100 cm^{-1}) and hydroxyl (OH^-) bands (around 3248 cm^{-1}) will show shifts and changes in intensity [8-10, 19, 20].

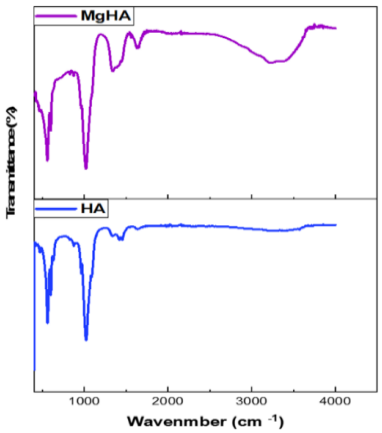


Fig. 3 – FTIR spectra of the HA and MgHA samples

Table 1 – The Characteristic bands of HA & MgHA in the FTIR spectrum

Sl. No.	Wavenumber	Band
1	3248 cm^{-1}	–OH stretching vibrations of adsorbed water
2	1420 cm^{-1}	Asymmetric Stretching of CO_3^{2-}
3	1021 cm^{-1}	Asymmetric Stretching PO_4^{3-}
4	961 cm^{-1}	Symmetric stretching of PO_4^{3-}
5	630 cm^{-1}	Stretching vibration of OH^- ions
6	600 cm^{-1}	In plane bending O–P–O in PO_4^{3-}
7	560 cm^{-1}	In plane bending O–P–O in PO_4^{3-}

3.3 EDX Analysis

EDX analysis of HA and MgHA samples is shown in Fig. 4 and Fig. 5. The Ca/P ratio for hydroxyapatite is found to be 1.77. When doping is done, the calcium-to-phosphorus ratio decreases, but the (Ca + Mg)/P ratio retains a value very close to 1.67 [2, 10]. For the MgHA sample, the (Ca + Mg)/P ratio is obtained as 1.74. These values are very close to the theoretical value of 1.67. This analysis also confirms the presence of magnesium in the sample.

Table 2 – The lattice constants, unit cell volume, crystallite size, and crystallinity of HA and MgHA samples

Sample	Crystallite Size (nm)	Lattice Constants (A^0)		Unit Cell Volume (A^{03})
		a = b	c	
HA	20.2	9.43	6.883	530.4
MgHA	15.7	9.42	6.880	529.6

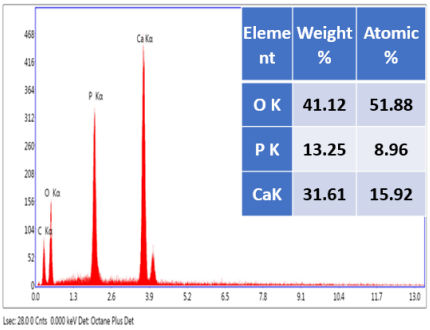


Fig. 4 – EDX spectrum of HA

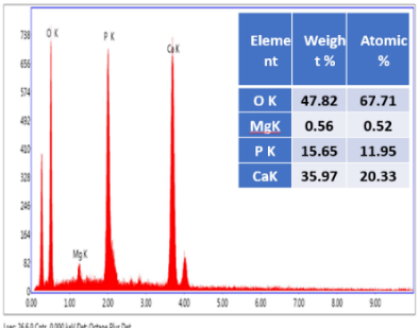


Fig. 5 – EDX spectrum of MgHA

3.4 Dielectric Analysis

The frequency-dependent dielectric feature of the sample was studied via broadband dielectric spectros-

copy. The dielectric characteristics of the samples were studied over a frequency range (1 Hz – 1 MHz). The real part of the dielectric constant (ε') is indicative of the stored energy in the dielectric. The variation of ε' and frequency is shown in Fig. 6. ε' is large at low frequency. This could be attributed to several factors, such as interfacial dislocations, charge defects, oxygen vacancies, grain boundary effects, and interfacial or space charge polarization [22]. A dielectric material is made up of conducting grains that are separated by insulating grain boundaries, according to the Maxwell-Wagner model. When an external field is applied, there is an action on charge carriers in the dielectric, which can usually move more easily across the grains; however, they tend to accumulate at the grain boundaries. The dielectric constant appears reasonably constant and flattens out in the high-frequency region because the atoms and electrons in the samples polarize fast and have high polarization with the application of the field [22]. Thus, the mobile ions cannot rotate fast enough, which means the dipoles' oscillation is lagging behind the applied field, and this lagging reduces the dielectric constant [22-25]. At high frequencies, the ionic, dipole, and space charge polarizations become ineffective [23]. This variation in dielectric constant with frequency is a characteristic of dielectric materials. The dielectric constant for 5mol% magnesium-doped hydroxyapatite is greater than that of pure hydroxyapatite because magnesium doping often leads to a decrease in grain size, and therefore, grain areas increase. This increases the Maxwell Wagner interfacial polarization as charge accumulates at the interface between the grains of different conductivities and dielectric properties. This interfacial polarization begins to dominate at low frequencies, which contribute to a high dielectric constant. When magnesium substitutes for calcium, the mismatch in lattice size drastically distorts the lattice and produces local point defects. As a result of local distortion, local dipoles are produced and result in increased polarizability of the material, especially at low and intermediate frequencies [22, 23, 26, 27].

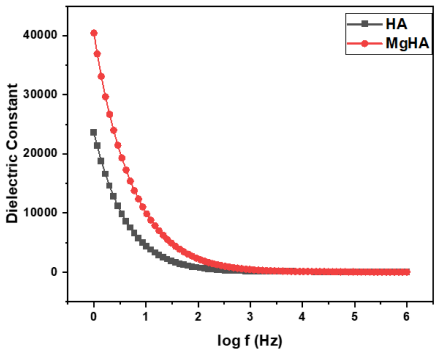


Fig. 6 – Variation of dielectric constant with frequency for HA and MgHA samples

Dielectric polarization occurs when a material is placed in an electric field. This indicates that the electric dipole moment of the material has changed by a process of polarization, as the dipoles have been aligned from random orientation to an orientation that is aligned with the applied electric field. The difference in phase between the electric field and dielectric polarization is termed "dielectric loss," which is an indication of the lost energy [22]. Fig. 7 depicts the change in dielectric loss with frequency for frequencies in the range of 1 Hz to 1 MHz. The dielectric loss decreases with an increase in frequency at low frequencies and reaches a plateau region at high frequencies. At low frequencies, the carriers are spatially confined, and the gradual movement of charge carriers is responsible for polarization in low frequencies. Hence, rotating dipoles in the low-frequency region requires more energy, resulting in high dielectric loss. At high frequency, charge carriers exhibit long-range mobility. One reason for the variation in dielectric properties is due to interfacial polarization from having phases with different conductivity [23]. The orientation of the hydroxyl ion (OH^-) will also induce a phase change in the materials. In addition, the host material, having a hexagonal structure, accommodates the incorporation of a variety of monovalent, divalent, and trivalent ion dopants within the hydroxyapatite lattice, which will influence the dielectric properties of hydroxyapatite [23]. The obtained results from our study indicated that the ion dopants in the host lattice shrink the structure, produce crystallographic defects, and increase the mobility of the charge carriers [23]. Thus, it is apparent that doping influences the dielectric properties. Materials with high dielectric loss offer good potential candidates for microelectronic system applications, energy storage, multilayer ceramic capacitors, and high-density energy storage industries [22].

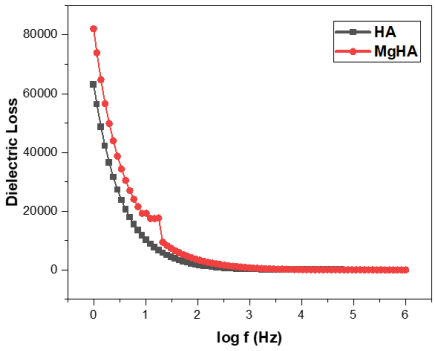


Fig. 7 – Variation of dielectric loss with frequency for HA and MgHA samples

Fig. 8 presents a frequency plot of the AC conductivity. The frequency dependence of conductivity is the sum of the DC conductivity due to free charge and the polarization conductivity due to bound charge. It can be seen from the figure that conductivity is increasing smoothly with frequency. The electrode polarization effects are present in the DC conductivity plateau region and disappear in the dispersive region at higher frequencies. Very low conductivity values at low frequencies may stem from ionic accumulation effects experienced from the slow periodic reversal of the electric field. In the high-frequency or mid-frequency region, features of Jonscher's power law nature emerge, and the conductivity increase is rapid with frequency (22-24). The mechanism demonstrates non-Debye relaxation processes, which show movement of charge carriers in the localized states [26]. The higher AC conductivity in Mg-doped Hydroxyapatite compared to

pure HA in broadband dielectric spectroscopy is mainly due to ionic mobility capacity and defect concentration enhanced by Mg substitution. Hence, because of an electric field, the mobility of the charge carriers (ions) is higher, which accounts for the higher conductivity, especially at higher frequencies [24].

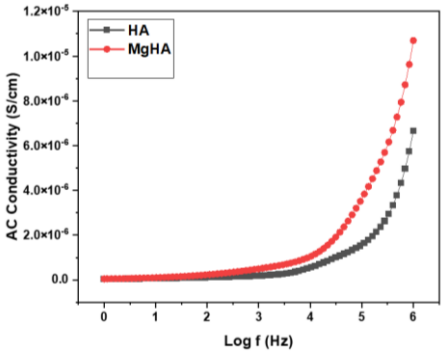


Fig. 8 – Variation of AC Conductivity with frequency for HA and MgHA samples

The capacitance decreases exponentially with increasing frequency (Fig. 9). An increasing frequency would promote the charge-transfer process that leads to capacitance decay [54]. Thus, the capacitance decays for both samples in the high-frequency range that follows conductivity. The capacitance of magnesium-doped hydroxyapatite is higher compared to the pure sample because magnesium doping introduces more mobile ions, which can shift and reorient under an electric field, leading to increased polarization and higher capacitance. Moreover, defects (vacancies, interstitials) that exist in the Mg-doped hydroxyapatite lattice can be charge traps or charge storage sites. This potentially enhances the capability of the material for charge storage, providing for a larger capacitance. While greater conductivity may result in higher dielectric loss, it can also contribute to the greater charge storage capacity of the material, particularly at lower frequencies, when the behaviour of the material is like a capacitor [22, 26-27].

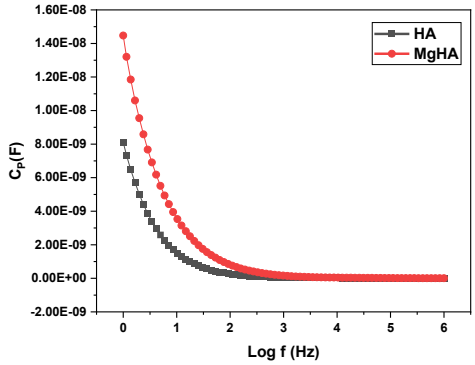


Fig. 9 – Variation of Capacitance with frequency for HA and MgHA samples

3.5 Measurement of Electrical Output

The peak-to-peak voltage and peak-to-peak current for the samples PVA, HA, and MgHA, and the obtained power density are given in Table 3. The output voltage for PVA, HA, and MgHA samples was found to be 220 ± 6 V, 261 ± 4 V, and 287 ± 6 V, respectively. The output current for the samples was found to be 6.8 ± 0.6 μA, 9.1 ± 0.4 μA, and 16 ± 0.7 μA, respectively. When the nanoparticles were added to PVA in the tribo-positive layer, the output increased. This is because the presence of nanoparticles enhances the surface roughness, dielectric properties, and effective surface area of the TENG [28-31]. The greater triboelectric performance from MgHA compared to pure HA can be attributed to several factors, including its dielectric constant, capacitance, charge trapping potential, and surface activity. Magnesium doping causes lattice strain and increases the dipole moment. Moreover, due to enhanced ion hopping, the AC conductivity also increases. These factors all increased surface charge density and improved electrical output, which may make MgHA a suitable candidate for biocompatible or flexible energy-harvesting applications, particularly as a constituent material for tribopositive layer in triboelectric nanogenerators [19].

Table 1 – Electrical output obtained for the samples

Sl. No.	Sample	VPP (V)	I PP (μA)
1	PVA	220 ± 6	6.8 ± 0.6
2	HA	261 ± 4	9.1 ± 0.4
3	MgHA	287 ± 6	16 ± 0.7

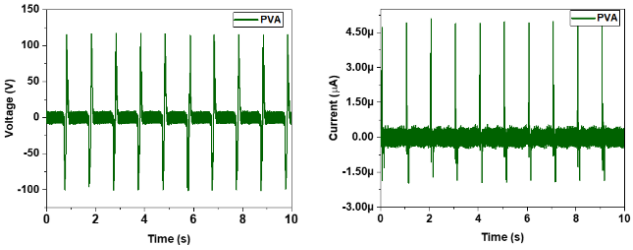


Fig. 10 – The variation of open circuit voltage and short circuit current of PVA

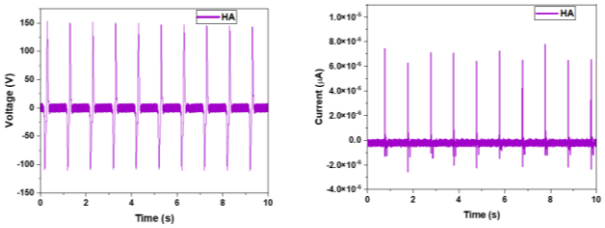


Fig. 11 – The variation of open circuit voltage and short circuit current of the HA-PVA layer

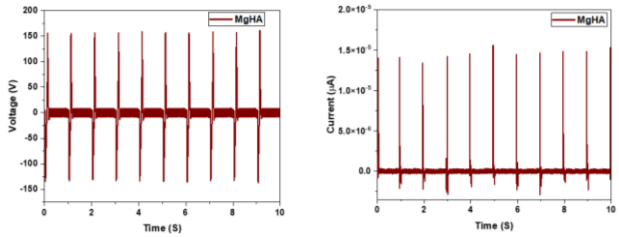


Fig. 12 – The variation of open circuit voltage and short circuit current of MgHA-PVA layer

4. CONCLUSION

This study presents an extensive investigation of

the dielectric behaviour of pure and magnesium-doped nanohydroxyapatite (MgHA) using broadband dielectric spectroscopy over a frequency range of 1 Hz to 1 MHz. The measured parameters – real permittivity (ε'), imaginary permittivity (ε''), AC conductivity (σ_{ac}), and capacitance (C_p) – were found to improve substantially in the MgHA samples compared to undoped hydroxyapatite. The rise in ε' for MgHA is a measure of the increased capacity to hold electrostatic energy, which is mainly attributed to defect-induced dipoles and interfacial polarization as a result of magnesium substitution. The higher ε'' is in line with increased dielectric relaxation and movement of charge carriers, which agrees with the seen increase in AC conductivity (σ_{ac}). These trends indicate that Mg doping provides localized charge carriers and defect dipoles that take an active role in polarization and conduction processes. The increased *Cp* values also indicate enhanced charge accumulation and capacitive performance, perhaps arising from increased dielectric surface area and grain boundary effects. Together, these improvements place MgHA as a high-permittivity bioceramic with promising applications in a wide variety of future technologies like dielectric energy storage devices, micro-capacitors, Triboelectric nanogenerators (TENGs), piezoelectric harvesters, and flexible electronic components. Overall, magnesium doping appears as a versatile method to modulate the dielectric and electrical performance of hydroxyapatite, rendering it an ideal material for next-generation bioceramic and energy-harvesting platforms.

ACKNOWLEDGEMENTS

The authors are grateful to the authorities of the Sophisticated Analytical Instrumental Facilities (SAIF), Cochin University of Science and Technology, and the CLIF, University of Kerala, for providing advanced instrumental and analytical facilities. The authors would like to thank the Principal, M G College, Thiruvananthapuram, and Advanced Tribology Research Centre, CET, for providing the facilities for doing this research.

DECLARATION OF COMPETING INTEREST

The authors declare that they have no known competing financial interests or personal relationships that could have appeared to influence the work reported in this paper.

DATA AVAILABILITY

Data will be made available on request.

AUTHORSHIP CONTRIBUTION STATEMENT

Sindhu R L: Conceptualisation, Methodology, Investigation, Formal analysis, interpretation of results, Writing – original draft.

Sini Chandran: Writing – original draft.

Anandakumar V M: Writing – review & editing, Supervision

REFERENCES

1. S Navalagunda B, P., *Int. J. Sci. Res.* (IJSR) **12**, 1620 (2023) https://doi.org/10.21275/SR23612172321.
2. N.A.S. Mohd Pu'ad, R.H. Abdul Haq, H. Mohd Noh, H.Z. Abdullah, M.I. Idris, T.C. Lee, *Mater. Today Proc.* **29**, 233 (2020) https://doi.org/10.1016/j.matpr.2020.05.536.
3. T.J. Webster, E.S. Ahn, *Tissue Engineering* II (Springer Berlin Heidelberg: n.d.) 275 (2006) https://doi.org/10.1007/10_021.
4. S. Bose, S. Vahabzadeh, A. Bandyopadhyay, *Mater. Today* **16**, 496 (2013) https://doi.org/10.1016/j.mattod.2013.11.017.
5. V. Uskoković, D.P. Uskoković, *J. Biomed. Mater. Res. Part B Appl. Biomater.* **96B**, 152 (2011) https://doi.org/10.1002/jbm.b.31746.
6. Z. Kubiak-Mihkelsoo, A. Kostrzębska, A. Błaszczyszyn, A. Pitułaj, M. Dominiak, T. Gedrange, I. Nawrot-Hadzik, J. Matys and J. Hadzik, *Appl. Sci.* **15**,1108 (2025) https://doi.org/10.3390/app15031108.
7. L. Duta, V. Grumezescu, *Materials* **17**, 640 (2024) https://doi.org/10.3390/ma17030640.
8. S. Ziani, S. Meski, H. Khireddine, *Int. J. Appl. Ceram. Technol.* **11**, 83 (2014) https://doi.org/10.1111/ijac.12093.
9. J. Singh, H. Singh, U. Batra, *Biomaterials Science: Processing, Properties, and Applications V.* 161 (2015) https://doi.org/10.1002/9781119190134.ch15
10. D. Predoi, S.L. Iconaru, M.V. Predoi, G.E. Stan, N. Buton, *Nanomaterials* **9**, 1295 (2019) https://doi.org/10.3390/nano9091295.
11. F. Miyaji, Y. Kono, Y. Suyama, *Mater. Res. Bull.* **40**, 209 (2005) https://doi.org/10.1016/j.materresbull.2004.10.020.
12. M.R. Senra, R.B. de Lima, D.D.H.S. Souza, M.F.V. Marques, S.N. Monteiro, *J. Mater. Res. Tecnol.* **9**, 7190 (2020) https://doi.org/10.1016/j.jmrt.2020.04.089.
13. S.C. Cox, P. Jamshidi, L.M. Grover, K.K. Mallick, *Mater. Sci. Eng. C* **35**, 106 (2014) https://doi.org/10.1016/j.msec.2013.10.015.
14. H. Zhang, C. Zhao, J. Wen, X. Li, L. Fu, *Silikáty* **61**, 244 (2017) https://doi.org/10.13168/cs.2017.0022.
15. I. Ullah, M.A. Siddiqui, S.K. Kolawole, H. Liu, J. Zhang, L. Ren, K. Yang, *Ceram. Int.* **46** 14448 (2020) https://doi.org/10.1016/j.ceramint.2020.02.242.
16. C.L. Popa, A. Deniaud, I. Michaud-Soret, R. Guégan, M. Motelica-Heino, D. Predoi, *J. Nanomater.* 1062878 (2016) https://doi.org/10.1155/2016/1062878.
17. G.D. Venkatasubbu, S. Ramasamy, V. Ramakrishnan, G.S. Avadhani, R. Thangavel, J. Kumar, *Int. J. Nanosci. Nanotechnol.* **2** 1 (2011).
18. A.T. Reda, T.G. Weldemhret, J.Y. Park, S. Lim, N.T. Debele, S.S. Choi, C. Cho, Y.T. Park, *Sensor. Actuat. A Phys.* **370**, 115197 (2024) https://doi.org/10.1016/j.sna.2024.115197.
19. M. Riaz, M. Najam, S. Arif, S. Farooq, A. Mahmood, *J. Mech. Behav. Biomed. Mater.* **142** 105830 (2023) https://doi.org/10.1016/j.jmbbm.2023.105830.
20. B. Yedekçi, A. Tezcaner, A.Z. Alshemary, B. Yılmaz, T. Demir, Z. Evis, *J. Mech. Behav. Biomed. Mater.* **115**, 104230 (2021) https://doi.org/10.1016/j.jmbbm.2020.104230.
21. J. Ran, P. Jiang, G. Sun, Z. Ma, J. Hu, X. Shen, H. Tong, *Mater. Chem. Front.* **1** 900 (2017) https://doi.org/10.1039/C6QM00192K.
22. S. Suresh, V.P.S. S., D. S., K.V.T. S., *Mater. Today Commun.* 36, 106657 (2023) https://doi.org/10.1016/J.MTCOMM.2023.106657.
23. S. Helen, A.R. Kumar, *Mater. Chem. Phys.* **237**, 121867 (2019) https://doi.org/10.1016/J.MATCHEMPHYS.2019.121867.

24. K.P. Tank, P. Sharma, D.K. Kanchan, M.J. Joshi, *Cryst. Res. Technol.* **46**, 1309 (2011) https://doi.org/10.1002/crat.201100080.
25. K.P. Tank, B.V. Jogiya, D.K. Kanchan, M.J. Joshi, *Solid State Phenom.* **209**, 151 (2013) https://doi.org/10.4028/www.scietific.net/SSP.209.151.
26. L. Sundarabharathi, M. Chinnaswamy, *J. Sol-Gel Sci. Technol.* **88**, 296 (2018) https://doi.org/10.1007/s10971-018-4802-z.
27. L. Sundarabharathi, D. Ponnamma, H. Parangusan, M. Chinnaswamy, M.A.A. Al-Maadeed, *SN Appl. Sci.* **2**, 94 (2020) https://doi.org/10.1007/s42452-019-1807-3.
28. N.D. Huynh, H.-W. Park, K.-B. Chung, D. Choi, *Curr. Opt. Photonics* **31**, 365 (2018) http://dx.doi.org/10.7234/coposres.2018.31.6.365.
29. R. Zhang, H. Olin, *ACS Nanosci. Au* **2**, 12 (2022) https://doi.org/10.1021/acsnanoscienceau.1c00026.
30. G. Zhu, Z.-H. Lin, Q. Jing, P. Bai, C. Pan, Y. Yang, Y. Zhou, Z.L. Wang, *Nano Lett.* **13,** 847 (2013) https://doi.org/10.1021/nl4001053.
31. H. Zhang, P. Zhang, P. Li et al., *Nano Res.* **15,** 7163 (2022) https://doi.org/10.1007/s12274-022-4326-2.
32. G. Khandelwal, N.P.M.J. Raj, S.-J. Kim, *Nano Today* **33**, 100882 (2020) https://doi.org/10.1016/j.nantod.2020.100882.

Вплив легування магнієм на діелектричні властивості та трибоелектричні характеристики наногідроксиапатиту

Sindhu R L[1,2,3], Sini Chandran[1,3], Ananda Kumar V M[1,3]

[1] *Mahatma Gandhi College, 695004 Thiruvananthapuram, Kerala, India*
[2] *University College, 695034 Thiruvananthapuram, Kerala, India*
[3] *University of Kerala, 695034 Thiruvananthapuram, Kerala, India*

Гідроксиапатит, біокераміка, що імітує мінеральний склад кістки, привернула увагу як in vitro, так і in vivo завдяки своїй чудовій біосумісності та остеопровідності. Чистий та легований магнієм гідроксиапатит був синтезований хімічним методом, а зразки були охарактеризовані за допомогою XRD, FTIR та EDX. Були виміряні діелектрична проникність, провідність змінного струму, діелектричні втрати та ємність зразків. Вивчення діелектричних властивостей матеріалів на основі гідроксиапатиту для біоелектроніки та інтелектуальних біомедичних пристроїв є нещодавньою сферою інтересу. Також були проведені попередні дослідження впливу цих зразків на трибоелектричні характеристики полівінілового спирту. Магній є важливим мікроелементом у кістках людини, тому його було включено до решітки наногідроксіапатиту для покращення біологічних характеристик та електричних властивостей. Результати вказують на можливість налаштування електричних властивостей наногідроксіапатиту та застосування наногідроксіапатиту, легованого магнієм, для майбутніх біомедичних пристроїв, сенсорів та пристроїв для збору енергії.

Ключові слова: Наногідроксиапатит, Хімічне осадження, Діелектричні втрати, Діелектрична проникність, Гідроксиапатит, легований магнієм, TENG.